PHYSICAL REVIEW C **83**, 024609 (2011)

Isomeric cross section of the ^{197}Au(n,2n) reaction

A. Tsinganis,[1,*] M. Diakaki,[1] M. Kokkoris,[1] A. Lagoyannis,[2] E. Mara,[1] C. T. Papadopoulos,[1] and R. Vlastou[1]
[1] *Department of Physics, National Technical University of Athens, Athens, Greece*
[2] *Institute of Nuclear Physics, National Centre of Scientific Research (NCSR) "Demokritos," Athens, Greece*

(Received 29 September 2010; published 25 February 2011)

In the present work, the ^{197}Au(n,2n) reaction cross section is experimentally determined relative to the ^{27}Al(n,α)^{24}Na reaction at incident neutron energies of 9.0–10.5 MeV by means of the activation technique. The quasimonoenergetic fast neutron beam was produced via the ^{2}H(d, n)^{3}He reaction at the 5.5-MV Tandem Van de Graaff accelerator at the National Centre of Scientific Research (NCSR) "Demokritos" and was studied to determine the contribution of background "parasitic" neutrons using the multiple foil activation technique and the SULSA unfolding code. The cross sections for the population of the second isomeric state (12^-) of ^{196}Au and the sum of the ground (2^-) and first isomeric state (5^-) population cross sections were independently determined. Auxiliary Monte Carlo simulations were performed with the MCNP code. Theoretical calculations of the above cross sections in the 8–25 MeV region were carried out with the use of the STAPRE-F, EMPIRE, and TALYS codes, which were also compared in their implementation of the generalized superfluid model. The theoretical results are compared with previous work in the same mass region, and the strong dependence on the level scheme of the nuclei involved was revealed.

DOI: 10.1103/PhysRevC.83.024609 PACS number(s): 24.10.−i, 24.60.Dr, 27.80.+w, 28.20.−v

I. INTRODUCTION

The presence of a high-spin isomeric state in the residual nucleus of a neutron threshold reaction provides a sensitive test for existing nuclear models. The study of such reactions is a powerful tool for obtaining information on the structure of nuclei. In particular, the nuclei of the transitional region from well deformed to spherical nuclei near the $Z = 82$ shell closure (Os-Pb region) present a very complex structure (γ softening, triaxiality, shape coexistence) and for most of them an isomer with a high-spin value with respect to the spin of the corresponding ground state has been reported. For the same element the energy of this isomer increases with increasing mass number A. Its existence is attributed to the coupling of high-spin intruder states, and the systematic study of the excitation function of the formation of both the ground and the high-spin isomeric state on the basis of a statistical model provides information on the energy and spin distribution of the level density of the nuclei involved [1] and on the changes in the structure of the low-lying excited states of the corresponding nuclei.

In this context the ^{196}Au isotope presents an interesting isomeric pair: ground and isomeric states with spin values of 2^- and 12^-, respectively (Fig. 1). This 12^- isomer has been reported for other even A Au isotopes (^{198}Au, ^{200}Au) [2]. However, a survey of the literature revealed only a limited number of experimental data for the cross section of the ^{197}Au(n,2n)^{196}Au^{m2} reaction, especially near its threshold, where only one unpublished dataset [3] was found.

Thus, the purpose of this work was to experimentally determine the ^{197}Au(n,2n)^{196}Au^{m2} and the ^{197}Au(n,2n)^{196}Au^{g+m1} reaction cross sections in the incident neutron energy range between 9 and 10.5 MeV, i.e., close to the threshold, by means of the activation technique. Additionally, theoretical statistical model calculations were performed and compared to all available experimental data over an extended energy range to study the contribution of the spin distribution and the details of the level scheme of the residual nucleus to the formation of the isomeric state.

II. EXPERIMENTAL

A. Irradiations

Four irradiations have been carried out, evenly spaced in the energy range between 9.0 and 10.5 MeV. Given that the cross section for the formation of the second isomeric state is significantly lower than that for the population of the ground state, the irradiations typically lasted ~24 h, which corresponds to roughly 84% of the saturated activity of the second isomeric state.

High-purity natural gold foils (99.99% ^{197}Au) with a diameter of 14 mm and thickness of 0.5 mm were used. Two Al foils of the same diameter and thickness were placed immediately before and after the gold foil and were used to determine the neutron flux.

The quasimonoenergetic neutron beam was produced via the ^{2}H(d,n)^{3}He reaction by bombarding a deuterium gas target with a deuteron beam at currents ~1–2 μA. The gas target is fitted with a 5-μm molybdenum entrance foil and a 1-mm Pt beam stop, and is constantly cooled with a cold air jet during irradiation to diminish the risk of damage to the Mo foil. The deuterium pressure was set to 1500 mbar. Using this setup, the achieved flux varied between 3×10^{5} and 4×10^{6} $n/(\mathrm{cm}^2\ \mathrm{s})$ in the four runs performed.

The samples were placed at 0° with respect to the neutron beam and at a distance of 8 cm from the center of the gas cell, thus limiting the angular acceptance of the target foils to ±5°.

Beam fluctuations were monitored with a BF_3 counter placed at a distance of 3 m from the deuterium gas target.

---

[*] tsiganis@mail.ntua.gr

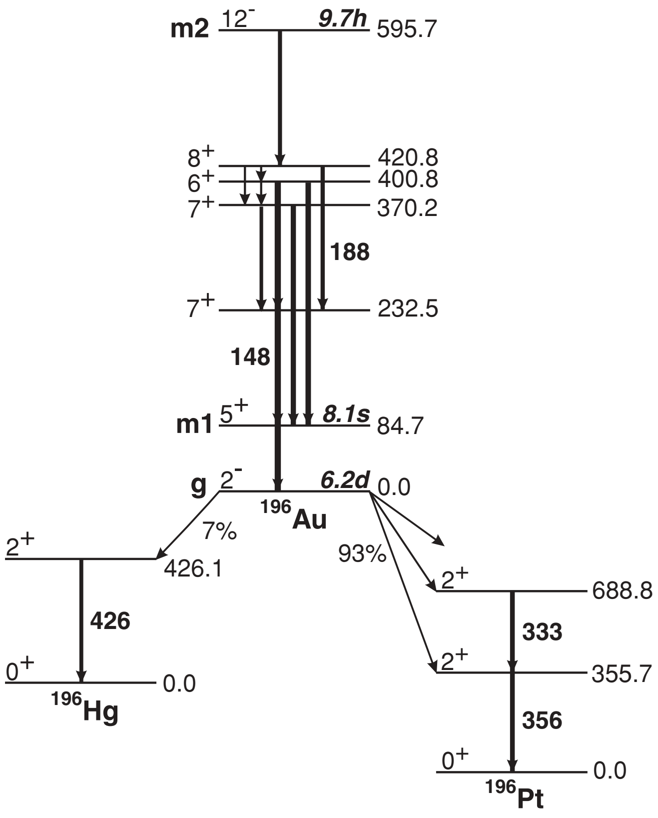

FIG. 1. Simplified decay scheme of the isomeric and ground states of the residual nucleus ^{196}Au. All energies are given in keV.

Following Monte Carlo simulations of the experimental area, the BF$_3$ unit was placed at an angle of 30° with respect to the beam line to avoid an increased presence of "parasitic" background neutrons near the target foils owing to backscattering on the BF$_3$ setup. Data from the BF$_3$ counter were stored at regular time intervals (60 s) by means of a multichannel scaler, and were used to correct for the decay of ^{196}Au nuclei during irradiation and to account for fluctuations in the beam flux in the subsequent off-line analysis.

The main quantities concerning the irradiations of the samples are summarized in Table I.

B. Neutron beam

Particular attention was given to estimating the neutron energy distribution in the samples. The linearity of the selection magnet has been verified at low energies through the Al(p,γ) strong resonance at 991.91 keV and the ^{16}O(d,n) threshold reaction ($E_{\mathrm{th}} = 1828.83$ keV), leading to an estimate of the beam energy offset of 1.6 keV and a beam energy uncertainty of 0.1%. Assuming possible nonlinearity at high energies, an overestimated beam energy uncertainty of 0.15% has been accepted to include possible second-order effects.

A considerably more significant effect on the energy uncertainty of the produced neutrons is straggling from energy loss in the entrance foil and the deuterium target. Furthermore, as it was not possible to control the flow of deuterium in the gas cell remotely, the pressure was at times lower than the desired value by up to 200–300 mbar. These effects were estimated with the SRIM software [4] and the energy uncertainty value from straggling was less than 30 keV. Finally, the angular acceptance of the target foils introduces additional uncertainty owing to the ^{2}H$(d,n)^3$He reaction kinematics.

Taking the above into account, the appropriate adjustments were made, where possible, to ensure that the width of the neutron energy distribution in the samples did not exceed 50 keV.

The contribution of background "parasitic" neutrons was also studied in detail. These neutrons originate from the interaction of the deuteron beam with the beam-line structural materials, beam collimators, and gas cell components. The multiple foil activation technique was implemented to determine the neutron beam profile. The appropriate foils were chosen in which neutron threshold reactions take place at different threshold energies, and they were placed immediately after the Au and two Al foils for irradiation. Information from the Au and Al foils was also included in this analysis. The relevant reactions with their threshold energies are presented in Table II.

The results of these irradiations were processed with the SULSA unfolding code [5]. A key feature of the code is that it does not require an input spectrum. By providing the activation rates measured for each foil, the code extrapolates the energy distribution of the beam by using cross-section values and covariance matrices from an incorporated library. Modifications were made to include additional reactions in the analysis.

TABLE I. Summary of the irradiation and off-line measurement parameters

	9.0 MeV	9.5 MeV	10.0 MeV	10.5 MeV
Irradiation time (h)	23.22	14.03	25.12	25.08
Integrated flux ($\times 10^{11}$) (cm^{-2})	3.45 ± 0.19	0.27 ± 0.02	4.62 ± 0.18	0.33 ± 0.02
Measurement time[a] (h)	10.96[b]/10.96	3.89/1.00	21.97/5.98	51.15/19.95
Decay correction f[a]	0.948/0.490	0.964/0.599	0.944/0.462	0.943/0.458
Decay correction D[a]	0.050/0.515	0.012/0.061	0.057/0.325	0.125/0.706

[a] Two values are given for these parameters: A/B. The A corresponds to the σ_{g+m1} and the B value to the σ_{m2} measurement.

[b] In this case, the contribution of the decay of the second isomeric state to the activity of the ground state was negligible owing to the very low cross section, and the measurements were carried out simultaneously.

TABLE II. Reactions used for neutron beam profiling.

	E_{th} (MeV)
^{58}Ni$(n,p)^{58}$Co	0.0
^{59}Co$(n,\alpha)^{56}$Mn	0.0
^{47}Ti$(n,p)^{47}$Sc	0.0
^{115}In$(n,n')^{115}$In^{m}	0.34
^{64}Zn$(n,p)^{64}$Cu	1.0
^{46}Ti$(n,p)^{46}$Sc^{g+m}	1.76
^{56}Fe$(n,p)^{56}$Mn	2.97
^{48}Ti$(n,p)^{48}$Sc	3.28
^{27}Al$(n,\alpha)^{24}$Na	3.25
^{197}Au$(n,2n)^{196}$Au	8.11
^{93}Nb$(n,2n)^{92}$Nb^{m}	8.93

The results of this analysis showed that, although a considerable population of background neutrons is produced during the irradiations, these lie mainly in the low-energy region, well below the threshold for the ^{197}Au$(n,2n)$ ($E_{\text{th}} = 8.11$ MeV) reaction. As far as the ^{27}Al$(n,\alpha)^{24}$Na reference reaction is concerned, while $E_{\text{th}} = 3.25$ MeV, the cross section only grows sufficiently to produce measurable activation rates at incident neutron energies above 6.8 MeV.

C. Activity measurements

Following the irradiations, the induced activity on the samples was measured with a 56% relative efficiency high-purity germanium (HPGe) detector. The detector was calibrated with ^{152}Eu and ^{207}Bi sources, the latter being used to obtain a more accurate efficiency curve in the low-energy region. The samples were placed at a distance of 10 cm from the detector window. With this counting setup, corrections for coincidence summing become negligible. Figure 2 shows typical spectra acquired from the gold samples during the measurement for the second isomeric state (top panel) and the ground state (bottom panel), where the γ rays of interest have been marked. The γ-ray intensities and half-lives used in the analysis are summarized in Table III.

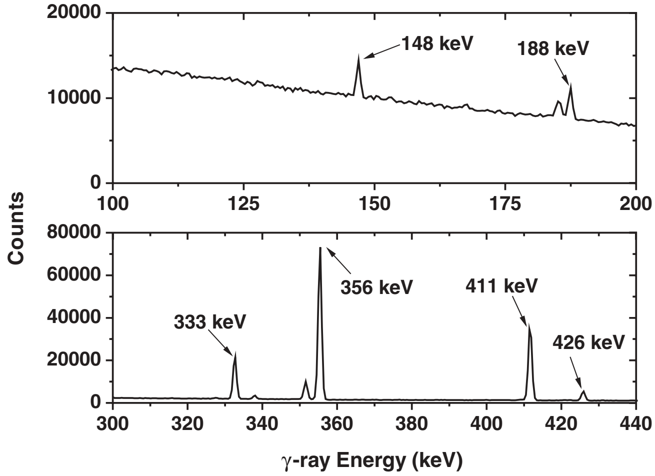

FIG. 2. Experimental spectra from the decay of the second isomeric state (top panel) and ground state (bottom panel) of ^{196}Au, after irradiation at 10.5-MeV incident neutron energy. The acquisition time is 20 and 51 h, respectively.

TABLE III. Decay properties of the daughter nuclei

Daughter nucleus	Half-life	γ-ray energy	Intensity per decay (%)
^{196}Au^{g}[a]	6.1669 ± 0.0006 d	333.0	22.9 ± 0.9
		355.7	87 ± 1
		426.1	6.6 ± 0.1
^{196}Au^{m2}[a]	9.6 ± 0.1 h	147.8	43.5 ± 0.1
		188.3	30.0 ± 1.5
^{24}Na[b]	14.9590 ± 0.0012 h	1368.6	100.0 ± 0.0

[a] Reference [6].
[b] Reference [7].

The population of the second isomeric state was measured through the 148-keV line. This was preferred over the 188-keV line owing to its higher intensity (45% over 30%) and the existence of a nearby natural background line (Fig. 2). These measurements began ∼1 h after the end of the irradiation and lasted up to 20 h (two half-lives), depending on the evolution of the peak-to-background ratio. Following this, the activity of the Al foils was measured with the same experimental setup through the 1369-keV transition. For these measurements, a duration between 1 and 3 h was sufficient to achieve a statistical error lower than 2%.

Because the first isomeric state decays relatively very quickly ($T_{1/2} = 8.1$ s), the measurements on the decay of the ground state result in the determination of the sum of the cross sections for the population of the ground state and the first isomeric state. Moreover, these measurements were carried out at least 2 days after the irradiation to ensure that the second isomeric state ($T_{1/2} = 9.6$ h) had fully decayed to the ground state, because the correction for the contribution of the second isomeric state to the measured activity of the ground state was found to be negligible when the latter measurement was carried out after several half-lives of the second isomeric state.

The activity of the ground state was deduced through the 356-keV line, preferred over the 333- and 426-keV lines owing to the much higher counting statistics (Fig. 2). Furthermore, the 333-keV line is contaminated by the 334-keV line of ^{198}Au arising from the ^{197}Au$(n,\gamma)^{198}$Au reaction. This is confirmed by the 411-keV line, which is clearly visible in the acquired spectrum and also belongs to the (n,γ) channel.

III. DATA ANALYSIS

In each case, the experimental values of the cross sections were determined through the following formula:

$$\sigma = \frac{N_\gamma}{\epsilon I N_T \Phi S f D}, \tag{1}$$

where N_γ is the number of counts in the relevant γ-ray peak. The factor ϵ is the detector efficiency, I is the γ-ray intensity, N_T is the number of target nuclei, and S is the self-absorption correction factor. Decays during irradiation and time fluctuations in the beam flux are accounted for with the correction factor f, given by

$$f = \frac{\int_0^{t_b} e^{-\lambda t} F(t)\, dt}{\int_0^{t_b} F(t)\, dt} e^{-\lambda t_b}, \tag{2}$$

where t_b is the irradiation time and $F(t)$ is the beam flux in arbitrary units as given by the BF_3 counter, while D corrects for the interval between the end of the irradiation and the end of the measurement and is given by

$$D = (1 - e^{-\lambda t_m})e^{-\lambda t_w}, \tag{3}$$

where t_w and t_m are the waiting time between irradiation and measurement and the measurement time, respectively.

The integrated neutron flux Φ was determined through the same formula Eq. (1)] by using the cross-section values for the $^{27}\mathrm{Al}(n,\alpha)^{24}\mathrm{Na}$ reaction found in literature [8] and by averaging over the deduced values in the front and back Al foils. It is thus possible to correct for target geometry and self-shielding.

Given the relatively low energy of the γ rays of interest and the high mass attenuation coefficient of gold, it was essential to take self-absorption effects into consideration. A Monte Carlo simulation of the counting geometry using the MCNP code [9] was performed to estimate this correction. Approximately 55% of the 148-keV line and 12% of the 356-keV line are lost owing to self-absorption in a 0.5-mm-thick gold foil. Self-absorption of the 1369-keV line in Al was found to be less than 0.5%.

The experimental uncertainties of all the factors used in Eq. (1) were summed quadratically in order to obtain the total cross section errors, and are summarized in Table IV.

IV. THEORETICAL CALCULATIONS

Theoretical cross-section calculations in the energy region between 8 and 25 MeV were performed, taking into account the compound and precompound nuclear processes, in the framework of the Hauser-Feshbach theory [10] and the exciton model [11], respectively. The level densities of the nuclei involved in the calculations were treated within the generalized superfluid model (GSM) in its phenomenological version developed by Ignatyuk *et al.* [12,13], which takes into account superconductive pairing correlations, shell effects, and collective enhancement of the level density of the nucleus in a consistent way. It has already been used successfully in the past for theoretical cross-section calculations in ^{191}Ir [14], which also lies in the transitional Os-Pb region.

TABLE IV. Experimental uncertainties.

	Uncertainty (%)
Neutron energy	<1
Neutron flux[a]	4 – 6.5
Correction factors	2
Time factors	<0.5
Counting statistics[b]	0.2–1.2/4.2–15.1[c]
γ-ray intensity per decay[b]	1.1/0.2
Detector efficiency	5
Total uncertainty of cross section	7.3–8.7/8.3–17.7[c]

[a] Including 2% uncertainty in the $^{27}\mathrm{Al}(n,\alpha)^{24}\mathrm{Na}$ cross section.

[b] Two values are given for these parameters: A/B. The A corresponds to the σ_{g+m1} and the B value to the σ_{m2} measurement.

[c] The value of the counting statistics uncertainty is 41.5% for the 9.5-MeV run, owing to the low beam current and shorter than desired irradiation, leading to a total cross-section uncertainty of 42.4%.

Within the GSM, the level density $\varrho(U, J)$ is treated separately in two energy regions depending on the nuclear temperature t. The critical nuclear temperature value t_{cr} is given by $t_{\mathrm{cr}} = 0.567\Delta_0$, where $\Delta_0 = 12/\sqrt{A}$ is the pairing correlation function. For $t < t_{\mathrm{cr}}$ (or $U' < U_{\mathrm{cr}}$) the nucleus is in the superfluid phase, where $\rho(U')$ is the level density of quasiparticle excitations in the Bardeen-Cooper-Schrieffer (BCS) theory [15], expressed in terms of the effective excitation energy $U' = U + n\Delta_0$, where U is the true excitation energy of the compound nucleus and $n = 0, 1, 2$ for even-even, even-odd, and odd-odd nuclei. The level-density parameter is considered constant in the superfluid phase of the nucleus.

For $t \geqslant t_{\mathrm{cr}}$ (or $U' \geqslant U_{\mathrm{cr}}$) the nucleus is in the normal phase, where the pairing correlations vanish and the level density follows the simple parametrization of the Fermi gas model [16] with a shift in the excitation energy by $E_{\mathrm{cond}} = (3/2\pi^2)\alpha_{\mathrm{cr}}\Delta_0^2$, which is the condensation energy characterizing the decrease of the ground state of the Fermi gas because of the correlation interaction. The level-density parameter α varies with energy according to the equation

$$\alpha = \tilde{\alpha}\left[1 + \frac{\delta\epsilon_0}{U' - E_{\mathrm{cond}}} f(U' - E_{\mathrm{cond}})\right], \tag{4}$$

where $\tilde{\alpha}$ is the asymptotic value of α at high excitation energy and $\delta\epsilon_0$ is the shell correction of the nuclear binding energy. The dimensionless function $f(U')$ determines the energy behavior of α for the normal phase [13].

The calculations were carried out using three codes, STAPRE-F [17], EMPIRE 2.19 [18], and TALYS-1.2 [19]. Some important details on each are given below.

A. STAPRE-F calculations

The STAPRE-F code is designed to estimate energy-averaged cross sections for particle-induced reactions with several possible emitted particles (n, p, α, d) and γ rays, under the assumption of sequential evaporation. For each evaporation step the statistical model is used with respect to energy, angular momentum, and parity conservation. In the present work, only the contribution of neutrons and γ rays was taken into account for the Hauser-Feshbach denominator because the charged particle emission is inhibited by the Coulomb barrier.

The neutron transmission coefficients were calculated using the ECIS03 code [20] with the global optical model parameters by Koning and Delaroche [21], as the gold isotopes in question are slightly deformed (as indicated by the quadrupole deformation parameter ε in Table V).

For the first evaporation step, preequilibrium decay is taken into consideration within the context of the exciton model. The preequilibrium emission factor is determined by the square matrix element $|M|^2 = KA^{-3}E^{-1}$, where A is the mass

TABLE V. Statistical model calculation parameters for STAPRE-F.

Parameter	^{198}Au	^{197}Au	^{196}Au	^{195}Au	Ref.
$\tilde{\alpha}$ (MeV^{-1})	16.827	16.736	16.645	16.554	[22]
$n\Delta_0$	1.706	0.855	1.714	0.859	[17]
$\delta\epsilon_0$	−4.392	−3.580	−2.931	−2.292	[22], [23]
ϵ, quadrupole deformation parameter	−0.131	−0.131	−0.139	−0.139	[24]
Neutron separation energy (MeV)	6.45	8.07	6.64	8.38	[25]
Average experimental total radiation width (meV)	128	120[a]	93[a]	70[a]	[22]

[a] These values were not included to the average parameters of s- and p- wave neutron resonances provided by A. V. Ignatyuk, and were deduced according to the neighboring nuclei values.

number of the target nucleus, E is the energy of the incident particle, and K is the free parameter of the model, which can be estimated by the hard component of the inelastically scattered neutrons or from the shape of the excitation function of $(n,2n)$ or $(n,3n)$ reactions. In the present work, the value of 200 was used for K.

The γ-ray strength functions for $M1$, $E2$, $M2$, and $E3$ were calculated according to the Weisskopf model, based on the single-particle estimation and normalized to the $E1$ strength function, which was calculated according to the Brink-Axel hypothesis [26,27]. The $E1$ strength function was normalized to reproduce the experimentally observed average radiation width $\langle\Gamma_\gamma\rangle$ at the neutron binding energy [22].

The GSM parameters used in the calculations were taken from literature and are summarized in Table V. For the perpendicular moment of inertia of the ground state of the nuclei involved, the empirical estimate $\Theta_{\rm rig}/3$ was used in consistency with the ground-state rotational bands of ^{196}Pt and ^{196}Hg.

The energies, spins, parities, and branching ratios of the discrete levels for each nucleus involved were taken from Nuclear Data Sheets [6], and the first 90 levels of ^{196}Au were included (up to ∼0.730 MeV). For the levels with unknown spin and parity, estimates from neighboring levels were made, while for levels with more than one spin assignment, a choice was made in order to include a variety of spin values.

B. EMPIRE calculations

EMPIRE-II is a modular system of nuclear reaction codes, implementing the major reaction mechanisms, such as compound nucleus (in the Hauser-Feshbach model with width fluctuation correction [28]), preequilibrium emission (by means of the exciton model or the hybrid Monte Carlo simulation approach) and direct interaction [using various optical model parameters automatically retrieved from the Reference Input Parameter Library (RIPL-2) library [22] or chosen by the user]. In the present work, version 2.19 was used with the default parameters concerning nuclear masses, ground-state deformations, discrete levels, decay schemes, and strength functions.

The emission of neutrons, protons, and α particles is automatically taken into account in competition with full γ cascade in the residual nuclei. The particle transmission coefficients were calculated using the ECIS03 code [20], using the optical model parameters by Koning and Delaroche [21] for neutrons and protons and the default parameters of [29] for α particles. The preequilibrium contribution was taken into account via the exciton model as implemented in the EMPIRE-II code (DEGAS) [18].

For the description of the level density in the continuum, the so-called dynamic approach of EMPIRE-II was used. This includes the superfluid model formalism [12] adjusted to experimental values of the level-density parameter α and to discrete levels for $U' < U_{\rm cr}$, and the Fermi gas model above $U_{\rm cr}$.

C. TALYS calculations

The TALYS-1.2 code is also a modular system of a variety of nuclear models for direct, compound, preequilibrium and fission reactions, phenomenological and microscopic level-density models, and automatic reference to libraries (RIPL-2 [22]) for the nuclear structure parameters needed in the calculations. All the reaction chains are followed until all possible exit channels are closed, leading to their ground or an isomeric state.

The default values were used for parameters concerning nuclear masses, ground-state deformations, discrete levels (except for the number of discrete levels included in the Hauser-Feshbach calculations, which was increased to accommodate the second isomeric state of ^{196}Au), decay schemes, and strength functions [26,27,30].

The particle transmission coefficients were calculated via the ECIS-06 code [20] using the default optical model parameters by Koning and Delaroche [21]. The preequilibrium contribution in the first step of the nuclear reaction was calculated via the default exciton model incorporated in TALYS [31]. The GSM level densities were selected with all the default parameters of the code. The explicit collective enhancement of the level density was enabled, and the level-density parameters were taken from the systematics for reasons of consistency with the other codes.

The above choices for the transmission coefficients, the preequilibrium, and the level densities used for the calculations of the three codes were made in order to compare how the three codes implement the generalized superfluid model. The STAPRE-F code provides a local approach in which a consistent calculation is made using local model parameters established on the basis of various independent data, while

TABLE VI. Experimental cross-section values for the ^{197}Au$(n,2n)^{196}$Au^{g+m1} and ^{197}Au$(n,2n)^{196}$Au^{m2} reactions and the isomeric cross-section ratio.

Energy (MeV)	σ_{g+m1} (mb)	σ_{m2} (mb)	$\sigma_{m2}/\sigma_{g+m1}$
9.0	328 ± 26	0.8 ± 0.1	0.0024 ± 0.0003
9.5	695 ± 60	8.9 ± 3.8	0.013 ± 0.006
10.0	1052 ± 73	16.2 ± 1.6	0.015 ± 0.002
10.5	1404 ± 102	32.8 ± 2.7	0.023 ± 0.003

EMPIRE and TALYS provide global approaches of the nuclear models included [32,33].

V. RESULTS AND DISCUSSION

The experimental results of this work are presented in Table VI along with their uncertainties. As seen in Fig. 3, the data for the ^{197}Au$(n,2n)^{196}$Au^{g+m1} cross section are in good agreement with previous measurements.

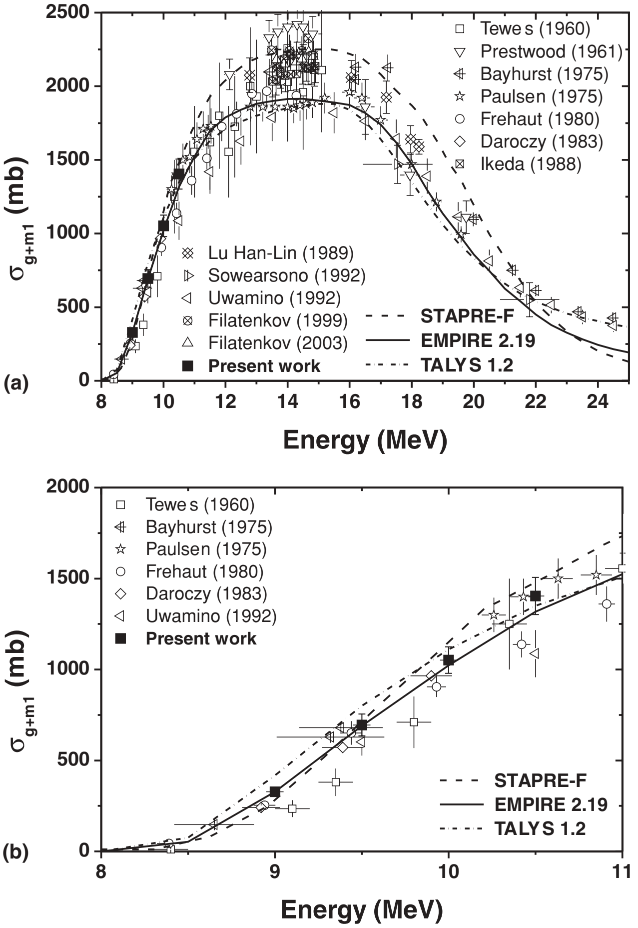

FIG. 3. Experimental values and theoretical calculations for the population of the ground and first isomeric state of ^{196}Au $(g+m1)$ between (a) 8 and 25 MeV and (b) 8 and 11 MeV. Several single-point datasets at ~14 MeV omitted for clarity.

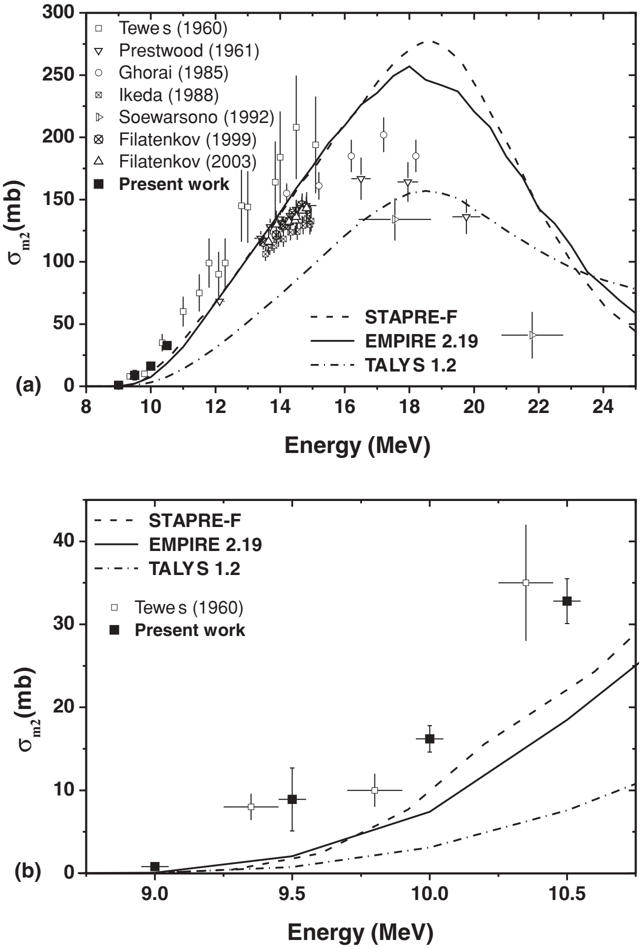

FIG. 4. Experimental values and theoretical calculations for the population of the second isomeric state of ^{196}Au $(m2)$ between (a) 8 and 25 MeV and (b) 8.5 and 11 MeV.

For the second isomeric state, only one previous dataset exists in the energy region from threshold to 13 MeV, contained in an unpublished report [3]. It has been impossible to obtain relevant information on the particular experiment, such as beam parameters, flux, irradiation intervals, and the detector(s) used for the off-line measurements. A dataset of evaluated data in this region can additionally be found in Ref. [34], also an unpublished report. The new data presented in this work report significantly lower uncertainties (10%–11% for the 10.0- and 10.5-MeV measurements compared to 20% in the other data within this range), barring the nonoptimal 9.5-MeV measurement. Moreover, the measurement at 9.0 MeV is the only one carried out at this energy, so close to the threshold. The uncertainty in the incident neutron energy has also been reduced compared to the previous data, as described in Sec. II B.

The theoretical calculations obtained from the three codes for σ_{g+m1} and σ_{m2}, along with the data from this work and the previous measurements are presented in Figs. 3 and 4.

As seen in Fig. 3, the results from all three codes fairly reproduce the trend of the experimental data for σ_{g+m1}. The theoretical curves appear to span the whole range of the experimental values in the 12–16 MeV region, where large discrepancies in the data exist. This precludes a conclusion on the accuracy of the results in this region.

Concerning the cross section of the second isomeric state (Fig. 4) the STAPRE-F and EMPIRE theoretical calculations seem to underestimate the near-threshold data up to ∼13 MeV, while in the high-energy region they overestimate the cross sections by ∼100 mb, despite the large discrepancies among the experimental data. The TALYS calculation underestimates the data in the whole energy range, a behavior also encountered in Ref. [32]. Furthermore, in all cases the cross section attains its maximum value at ∼18 MeV, ∼2 MeV higher than the experimental data suggests. This result will be discussed later. Nevertheless, all three codes reproduce the general trend of the experimental data.

Based on these observations, several tests were made, using the STAPRE-F code, to better reproduce the isomeric cross section results by changing the input parameters of the theoretical calculations and accounting for the $(n,3n)$ reaction, which becomes important above 16 MeV [35–37]. Particular attention was given to the value of $\tilde{\alpha}$ (Table V), which is the level-density parameter at high excitation energies [Eq. (4)] and plays an important role in the calculations.

Initially, these values were changed in a consistent way within their experimental uncertainties (i.e., ±6%) for $^{195-198}$Au isotopes. Subsequently, the $\tilde{\alpha}$ values for these isotopes were changed in order to follow the systematics proposed in (Ref. [22], p. 103), where α at the neutron separation energy is up to 20% lower than those given by Eq. (4) and decreases with increasing A.

Nevertheless, none of these attempts seemed to simultaneously improve the fit to the experimental data of σ_{m2}, σ_{g+m1}, and the cross-section values of the $(n,3n)$ reaction. Furthermore, the average experimental total radiation width and the moment of inertia of the ground state were changed within their experimental uncertainties, as was the percentage of preequilibrium emission and the assumptions on the shape and symmetry of the Au isotopes, but the effect on σ_{m2} was within 10%, and the theoretical curve remained shifted to higher energies.

Another test was made in order to understand and correct the shift of the σ_{m2} theoretical curve, which is shifted to higher energies compared to the experimental data as mentioned before. More specifically, the calculations were repeated using the back-shifted Fermi gas [38] and the Gilbert-Cameron level-density models [39] with the EMPIRE code, leaving the rest of the input parameters as mentioned above. The results (Fig. 5) show that the shift of the isomeric cross section curve is independent on the model of the level density of the nuclei involved. In addition, it can be seen in Fig. 4 that it is also independent on the implementation of the GSM in the three codes used.

Generally, the population of the high-spin isomers is highly dependent on the spin distribution of the continuum. The effect of this factor on the feeding of the 12$^-$ isomer was examined in order to improve the theoretical predictions.

In previous cross-section measurements of high-spin isomers in nuclei belonging to the transitional region from the well-deformed Os to the spherical Pb isotopes [14,40–42], the need of the reduction of the effective moment of inertia was pointed out in order to better reproduce the data of σ_{m2} and the isomeric ratio. Furthermore, in the framework of the back-shifted Fermi gas model (BSFGM), systematics have been evaluated for the mass dependence of the reduction of the effective moment of inertia with respect to the rigid-body value [43], which have been proved quite satisfactory in an extended mass region, even in the heavy Hg and Au isotopes [40]. The same result has occurred in the framework of the GSM for the Ir isotopes as reported in Ref. [14], where the effective moment of inertia had to be reduced to 75% of the rigid-body value in order to better reproduce the trend of the data. The BSFGM and GSM have the same spin distribution shape, and from the previous discussion one would also expect a similar systematic behavior of the spin cutoff parameter within the GSM, i.e., the need for a similar reduction of the effective moment of inertia for the reproduction of the data for Au. In order to test this idea, theoretical calculations were carried out using Θ_{eff} values lowered by 25% and 50% using the STAPRE-F and EMPIRE codes, and the results are presented in Fig. 6. The reduction of the effective moment of inertia causes a significant decrease of the isomeric cross section but does not seem to improve the theoretical results with reference

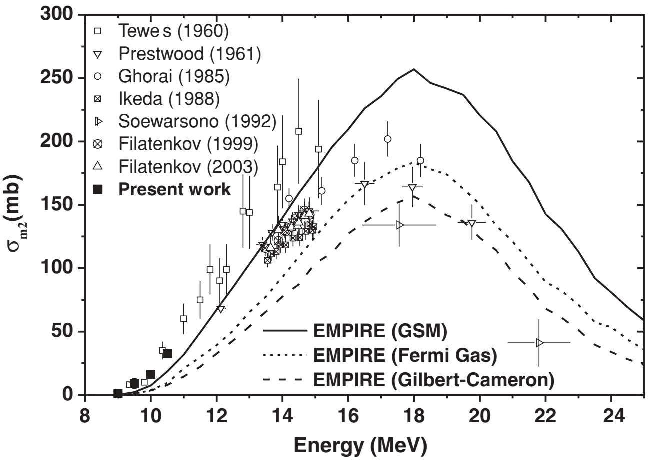

FIG. 5. Theoretical calculations for σ_{m2} using the Fermi gas and Gilbert-Cameron level-density models, compared to the result using the GSM.

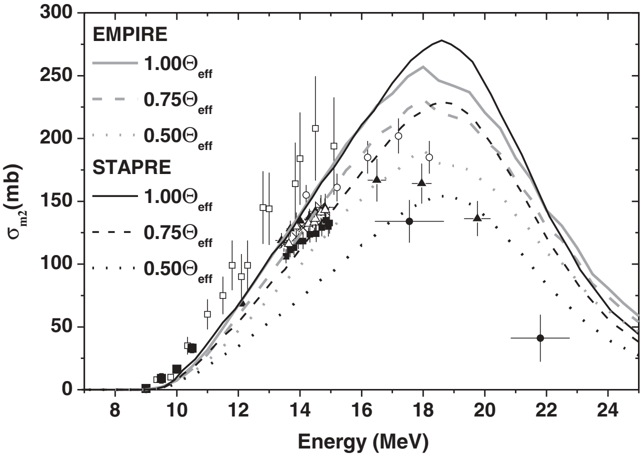

FIG. 6. Theoretical calculations for σ_{m2} using values of the effective moment of inertia reduced by 25% and 50%.

to the experimental data, as in the neutron energy region below 14 MeV the theoretical calculations are already lower than the experimental data, and as a result the lowering of Θ_{eff} causes a further deviation from the data. In the high-energy region the theoretical predictions move closer to the experimental data but retain the maximum cross-section value at ∼18 MeV in contrast with the data.

This result indicates that the reduced value of Θ_{eff} cannot improve the theoretical results and, given also the existing shift of the curve to higher energies, the hypothesis of possible discrepancies in the level scheme was examined. In particular, the level schemes of ^{196}Au and ^{195}Au are expected to play a crucial role in the cross-section value of the 12^- isomer and are discussed below.

The level scheme of ^{196}Au, especially the spins of levels lying above the 12^- isomer are very important for the feeding of this level [44,45] in the whole neutron energy range. The existence of the 12^- isomer among the low-lying excited states results from the high-spin intruder configurations $\pi h11/2 \otimes \nu i13/2$ [1] and inhibits its communication with neighboring states. The possible existence of a rotational band built on this intrinsic structure for doubly odd nuclei in this region is proposed in Refs. [46] and [47], and rotational bands based on high-j unique parity quasiparticle states ($\pi h9/2$, $\pi h11/2$, $\nu i13/2$) have been reported for Tl isotopes in Ref. [46] and other isotopes in the transitional region Os-Pb (references in Ref. [47]), as well as dipole bands in Pb and Hg isotopes [48–51]. The possible existence of a rotational band built on the 12^- isomer and feeding it through a gamma cascade would increase the calculated cross section, and lead to a better reproduction of σ_{m2} at incident neutron energies below 16 MeV. In a similar case, the existence of a rotational band built on the configuration of the 16^+ isomer of ^{178}Hf has been proposed in Ref. [45] in order to successfully reproduce, within the Hauser-Feshbach theory, the cross-section values of the ^{179}Hf$(n,2n)$ reaction that leads to its formation and was experimentally observed some years later via the incomplete fusion ^{176}Yb(^{9}Be,$\alpha 3n$) ^{178}Hf reaction [52].

The level scheme of ^{195}Au is also expected to play an important role in the neutron energy region above 16 MeV, where the $(n,3n)$ channel becomes important and where the largest deviation from the experimental data occurs. An examination of the level scheme of ^{195}Au in comparison with the level schemes of neighboring odd Au isotopes [53–55] indicates a possible absence of high-spin rotational band members from the documented levels. More precisely, in the level schemes of both ^{189}Au and ^{191}Au, $\Delta J = 2$ rotational band members have been observed, with spins from $\frac{11}{2}^-$ to $\frac{55}{2}^-$, energies up to ∼6 MeV and a band crossing at approximately $\frac{31}{2}^-$, following a systematic trend. The same trend is followed by reported levels of ^{193}Au up to the energy of 4 MeV, while for ^{195}Au only the first three states are reported (with spins up to $\frac{19}{2}^-$ and energies up to 1.5 MeV). The introduction of such high-spin states in the level scheme of ^{195}Au would lead to an increase of the deexcitation of the continuum of ^{196}Au toward these states, and thus a reduction of the theoretical σ_{m2} values above an incident neutron energy of 16 MeV.

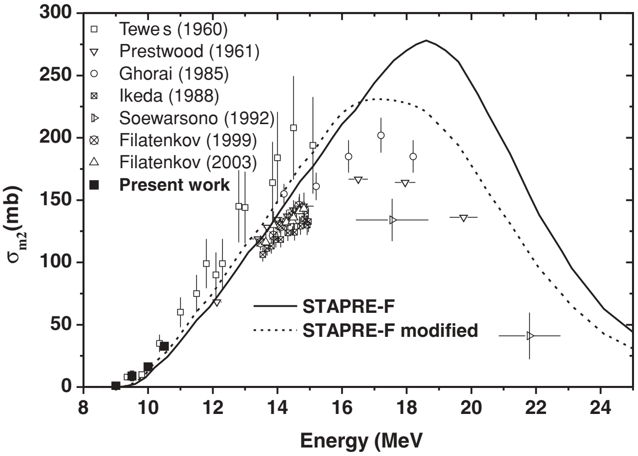

FIG. 7. Theoretical calculations for σ_{m2} using a modified level scheme for ^{196}Au and ^{195}Au including hypothetical high-spin levels.

Although the above assumptions on the level schemes of ^{196}Au and ^{195}Au seem physically likely, there is no possibility of embedding discrete levels in the continuum of the nuclei of interest via any of the three codes in order to further investigate this hypothesis and extract safe results.

The only test that could be performed was the addition of a few high-spin levels in the discrete via the STAPRE-F code implementation and the results seemed encouraging. More specifically, as far as the level scheme of ^{196}Au is concerned, several levels with spins $12^{\pm}$,$13^{\pm}$,$14^{\pm}$ have been added above the 12^- isomer and up to ∼0.730 MeV where the continuum starts, feeding the isomer through a gamma cascade. The result was a 10% enhancement of σ_{m2} without altering the $g + m1$ and $(n,3n)$ cross section values. In addition, in order to improve the σ_{m2} values in the high-energy region, a further addition of levels with high spins between $\frac{17}{2}^-$ and $\frac{27}{2}^-$ in the discrete of ^{195}Au was tried, which simultaneously reduced the σ_{m2} by 10% in the energy region above 16 MeV, as expected, and moved the maximum of the curve toward lower energies. The results of these two tests are shown in Fig. 7. Higher spins than those used in the tests, attributed to rotational bands, are expected to lie in the higher-energy part of the continuum, which has a high-spin distribution and part of it deexcites by feeding them. However, within the implementation of a code, the introduction of such high-spin levels in the discrete is not expected to significantly affect the results, because their feeding from the high-spin distribution part of the continuum would be negligible owing to the large energy difference.

VI. CONCLUSIONS

The cross section of the $(n,2n)$ reaction on ^{197}Au, was measured independently for the population of the second isomeric state (σ_{m2}), and for the sum of the reaction cross section for the population of the ground and the first isomeric state (σ_{g+m1}). The cross-section values were determined by means of the activation technique in the incident neutron energy range 9.0–10.5 MeV. Theoretical calculations in the energy range 8–25 MeV were performed with the use of three different codes (STAPRE-F, EMPIRE 2.19, and TALYS-1.2), taking into account all available experimental data. The exciton model and Hauser-Feshbach theory were employed for the precompound and compound processes, respectively. The generalized superfluid model was chosen for the description of the level density of the nuclei involved. The σ_{g+m1} cross section was easily reproduced by the calculations, while for σ_{m2}, the theoretical results could only reproduce the general trend of the experimental data, with the distribution being shifted to higher energies. Several tests were performed to improve the theoretical predictions. The results of these tests reveal the importance of the level scheme of the residual nuclei and indicate the possibility of incomplete documentation of high-spin levels in the level schemes of ^{196}Au and ^{195}Au. Furthermore, they highlight certain limitations of the nuclear codes used, particularly regarding the embedding of discrete states in the continuum, which is not currently possible and affects the reproduction of high-spin isomeric cross sections.

ACKNOWLEDGMENTS

The present work was partially supported by the NTUA program for fundamental research PEVE-2008. The authors would also like to acknowledge the assistance of the accelerator staff at NCSR "Demokritos."

[1] Y. P. Gangrsky, N. N. Kolesnikov, V. G. Lukashik, and L. M. Melnikova, Phys. At. Nucl. **67**, 1227 (2004).
[2] E. Hagn and E. Zech, Nucl. Phys. A **373**, 256 (1982).
[3] H. A. Tewes, A. A. Caretto, A. E. Miller, and D. R. Nethaway, Tech. Rep. 6028, 1960 (unpublished) (data retrieved from EXFOR: www-nds.iaea.org/exfor).
[4] J. F. Ziegler, J. P. Biersack, and U. Littmark, *The Stopping and Range of Ions in Solids* (Pergamon, New York, 1985).
[5] S. Sudar, Tech. Rep. INDC(HUN)-026/L 1989 (unpublished).
[6] H. Xiaolong, Nucl. Data Sheets **108**, 1093 (2007).
[7] R. B. Firestone, Nucl. Data Sheets **108**, 2319 (2007).
[8] A. Carlson, R. Block, J. Briggs, E. Cheng, H. Huria, M. Zerkle, K. Kozier, A. Courcelle, V. Pronyaev, and S. van der Marck, Nucl. Data Sheets **107**, 2931 (2006).
[9] F. B. Brown *et al.*, Trans. Am. Nucl. Soc. **87**, 273 (2002).
[10] W. Hauser and H. Feshbach, Phys. Rev. **87**, 366 (1952).
[11] J. J. Griffin, Phys. Rev. Lett. **17**, 478 (1966).
[12] A. V. Ignatyuk, K. Istekov, and G. N. Smirenkin, Sov. J. Nucl. Phys. **29**, 450 (1979).
[13] A. V. Ignatyuk, J. L. Weil, S. Raman, and S. Kahane, Phys. Rev. C **47**, 1504 (1993).
[14] N. Patronis, C. T. Papadopoulos, S. Galanopoulos, M. Kokkoris, G. Perdikakis, R. Vlastou, A. Lagoyannis, and S. Harissopulos, Phys. Rev. C **75**, 034607 (2007).
[15] J. Bardeen, L. N. Cooper, and J. R. Schrieffer, Phys. Rev. **106**, 162 (1957).
[16] H. A. Bethe, Rev. Mod. Phys. **9**, 69 (1937).
[17] M. Uhl and B. Strohmaier, Tech. Rep. IRK-76/01, 1976 (unpublished).
[18] M. Herman, R. Capote, B. V. Carlson, P. Obložinský, M. Sin, A. Trkov, H. Wienke, and V. Zerkin, Nuclear Data Sheets **108**, 2655 (2007).
[19] *TALYS-1.0*, edited by O. Bersillon, F. Gunsing, E. Bauge, R. Jacqmin, and S. Leray (EDP Sciences, France, 2008).
[20] J. Raynal, CEA Tech. Rep. CEA-N-2772 1994 (unpublished).
[21] A. J. Koning and J. P. Delaroche, Nucl. Phys. **A713**, 231 (2003).
[22] T. Belgya *et al.*, Tech. Rep. IAEA-TECDOC-1506, 2006 (unpublished), available online at [http://www.nds.iaea.org/RIPL-2/].
[23] W. D. Myers and W. J. Swiatecki, Ark. Fiz. **36**, 343 (1967).
[24] P. Moller, J. R. Nix, W. D. Myers, and W. J. Swiatecki, At. Data Nucl. Data Tables **59**, 185 (1995).
[25] G. Audi, A. H. Wapstra, and C. Thibault, Nucl. Phys. A **729**, 337 (2003).
[26] D. M. Brink, Nucl. Phys. **4**, 215 (1957).
[27] P. Axel, Phys. Rev. **126**, 671 (1962).
[28] H. Hofmann, J. Richert, J. Tepel, and H. Weidenmuller, Ann. Phys. **90**, 403 (1975).
[29] L. McFadden and G. R. Satchler, Nucl. Phys. **84**, 177 (1966).
[30] J. Kopecky and M. Uhl, Phys. Rev. C **41**, 1941 (1990).
[31] A. Koning and M. Duijvestijn, Nucl. Phys. A **744**, 15 (2004).
[32] V. Avrigeanu, S. V. Chuvaev, R. Eichin, A. A. Filatenkov, R. A. Forrest, H. Freiesleben, M. Herman, A. J. Koning, and K. Seidel, Nucl. Phys. A **765**, 1 (2006).
[33] M. Avrigeanu, R. A. Forrest, F. L. Roman, and V. Avrigeanu, PHYSOR-2006, ANS Topical Meeting on Reactor Physics, Vancouver, BC, Canada (unpublished).
[34] C. Phillis and O. Bersillon, Tech. Rep. 4826, 1977 (unpublished) (data retrieved from EXFOR: www-nds.iaea.org/exfor).
[35] S. Iwasaki, M. Sakuma, K. Sugiyama, and N. Odano, Tech. Rep. JAERI-M-93-046, 1993 (unpublished).
[36] L. Hanlin, H. Jianzhou, F. Peiguo, C. Yunfeng, and Z. Wenrong, Tech. Rep. INDC(CPR)-16, 1989 (unpublished) (data retrieved from EXFOR: www-nds.iaea.org/exfor).
[37] B. P. Bayhurst, J. S. Gilmore, R. J. Prestwood, J. B. Wilhelmy, N. Jarmie, B. H. Erkkila, and R. A. Hardekopf, Phys. Rev. C **12**, 451 (1975).
[38] W. Dilg, W. Schantl, H. Vonach, and M. Uhl, Nucl. Phys. A **217**, 269 (1973).
[39] A. Gilbert and A. Cameron, Can. J. Phys. **43**, 1446 (1965).
[40] S. Sudar and S. M. Qaim, Phys. Rev. C **73**, 034613 (2006).
[41] M. Al-Abyad, S. Sudar, M. N. H. Comsan, and S. M. Qaim, Phys. Rev. C **73**, 064608 (2006).
[42] S. F. Mughabghab and C. Dunford, Phys. Rev. Lett. **81**, 4083 (1998).
[43] S. I. Al-Quraishi, S. M. Grimes, T. N. Massey, and D. A. Resler, Phys. Rev. C **67**, 015803 (2003).
[44] S. M. Qaim, A. Mushtaq and M. Uhl, Phys. Rev. C **38**, 645 (1988).
[45] M. B. Chadwick and P. G. Young, Nucl. Sci. Eng. **108**, 117 (1991).
[46] A. J. .Kreiner, M. Fenzl, S. Lunardi, and M. Mariscotti, Nucl. Phys. A **282**, 243 (1977).
[47] A. J. Kreiner, Z. Phys. A **288**, 373 (1978).
[48] E. F. Moore *et al.*, Phys. Rev. C **51**, 115 (1995).
[49] H. Hubel, Prog. Part. Nucl. Phys. **38**, 89 (1997).
[50] N. Fotiades *et al.*, J. Phys. G **21**, 911 (1995).
[51] N. Fotiades *et al.*, Z. Phys. A **354**, 169 (1996).

[52] S. M. Mullins, G. D. Dracoulis, A. P. Byrne, T. R. McGoram, S. Bayer, W. A. Seale, and F. G. Kondev, Phys. Lett. B **393**, 279 (1997).

[53] S. C. Wu and H. Niu, Nucl. Data Sheets **100**, 1 (2003).

[54] V. Vanin, N. Maidana, R. Castro, E. Achterberg, O. Capurro, and G. Marti, Nucl. Data Sheets **108**, 2393 (2007).

[55] E. Achterberg, O. A. Capurro, G. Marti, V. Vanin, and R. M. Castro, Nucl. Data Sheets **107**, 1 (2006).